Shape coexistence in ^{72}Se

R. Palit,[1] H. C. Jain,[1] P. K. Joshi,[1] J. A. Sheikh,[2] and Y. Sun[3,4]
[1]*Tata Institute of Fundamental Research, Mumbai 400 005, India*
[2]*Physik-Department, Technische Universität München, D-85747 Garching, Germany*
[3]*Department of Physics, Tsinghua University, Beijing 100084, People's Republic of China*
[4]*Department of Physics and Astronomy, University of Tennessee, Knoxville, Tennessee 37996*
(Received 2 August 2000; published 23 January 2001)

Lifetimes have been measured up to the 22^+ level in the yrast positive-parity band and up to the 13^- level in the negative-parity band in ^{72}Se using the line-shape analysis methods. The $B(E2)$ and Q_t values obtained from these measurements show a prolate shape stabilization along the yrast band with increasing spins. A noncollective behavior is obtained even at the moderate spins for the negative-parity band. These experimental results are compared with theoretical predictions of the EXCITED VAMPIR and the projected shell model.

DOI: 10.1103/PhysRevC.63.024313 PACS number(s): 21.10.Re, 21.60.Cs, 23.20.Lv, 27.50.+e

I. INTRODUCTION

The influence of competing energy gaps in the f-p-g shell region reflects itself through drastic changes in collective properties of neutron deficient, transitional nuclei with masses between 70 and 80. Calculations employing the Strutinsky method [1] with folded Yukawa potential including pairing effects show two minima in potential energy curves for the light Se, Kr, and Sr isotopes: one at a large prolate deformation with $\beta_2 \approx 0.35-0.40$ and the other at an oblate deformation with $\beta_2 \approx -0.30$. Energy of the oblate minimum is several hundred keV higher than the prolate minimum for $N,Z=38$, but decreases with neutron number to some hundred keV below the prolate minimum for systems with $N,Z=35,36$. Thus, the coexistence of prolate-oblate shapes dominates the structure of low-spin states in this mass region. One of the best examples is ^{72}Se that shows a vibrational behavior in the spectrum up to $I^\pi=6^+$ and merges into a rotational-type band for higher spins with constant moment of inertia and deformation $\beta_2 \approx 0.3$ [2–5]. The low-spin anomaly in the yrast bands of ^{70,74}Se is also well known and has been interpreted as mixing of two bands with different deformations. There are theoretical investigations [2,6] based on the interacting boson model (IBM) to explain the effect observed in ^{72,74}Se without any special assumption about the nuclear shape or shape coexistence. Bands with different deformations also coexist in the neighboring odd-N isotopes ^{71,73}Se [7,8].

More recently, the yrast bands of ^{70,72,74}Se have been investigated [9,10] up to spins of $I^\pi=16^+$, 28^+, and 22^+, respectively. In case of ^{70}Se, a well-deformed minimum competes with a noncollective structure for high spins with $I \geqslant 8$ and both of the structures persist up to $\hbar\omega \approx 1.2$ MeV. This result is supported by the observation of several noncollective states in the vicinity of and above the 8^+ level. A recent study of ^{74}Se [10] shows a deformed shape for the excited states with a considerable softness towards triaxiality. The structure study of high spin states in ^{72}Se is of considerable interest because of the varying shape evolutions at high spins in even-even Se isotopes. Earlier experiments [2,11] on ^{72}Se included lifetime measurements up to 14^+ state along the yrast band. Absence of any sharp backbending after the low-spin anomaly along the yrast band in ^{72}Se has been interpreted as arising due to a strong yrast-yrare interaction at prolate deformation, causing a gradual alignment of two quasiprotons and two quasineutrons. A systematic increase of the $B(E2)$ values for spins up to 14^+ has been observed [2] in ^{72}Se, contrary to the trend found in ^{74}Se. This behavior was understood by a soft triaxial rotor with large rotation-vibration coupling rather than a rigid axially symmetric or triaxial rotor. The IBM in the vibrational limit gave an excellent fit to energies of the yrast states ($4 \leqslant I \leqslant 14$) and the $B(E2)$ values could be reproduced within a factor of 3. Later, a detailed microscopic investigation was performed for high-spin states up to $I^\pi=22^+$ by the EXCITED VAMPIR [12]. The overall agreement between the available experimental data and the calculations was qualitatively reasonable for the $B(E2)$ values.

In the present work, the lifetimes of the levels of ^{72}Se up to $I^\pi=22^+$ along the yrast band (see Fig. 1 for level scheme [9]) are measured through the doppler shift attenuation method (DSAM) to understand the structure at higher spins and excitation energies. Experimental Q_t values are compared with the EXCITED VAMPIR and the projected shell model (PSM) [13] calculations to investigate the shape variation with increasing spin in the yrast positive-parity band in ^{72}Se. The negative-parity band shows very irregular behavior at higher spins, indicating the dominance of single-particle behavior. The loss of collectivity in the negative parity band is also studied through a measurement of lifetimes of the levels by the DSAM.

II. EXPERIMENTAL PROCEDURE AND RESULTS

Levels in ^{72}Se were populated in the ^{54}Fe(^{24}Mg,$\alpha 2p$) reaction where an ^{54}Fe target was bombarded with 104 MeV ^{24}Mg beam from the 14-UD pelletron accelerator at Tata Institute of Fundamental Research, Mumbai. The target was prepared by rolling a 540-μg/cm^2-thick ^{54}Fe foil onto a 9-mg/cm^2-thick gold backing used for stopping the recoiling ions produced in various reaction channels. γ rays emitted from the nuclear excited states were detected in 5 CS-HPGe detectors and a CS-Clover detector. γ-γ coincidence data

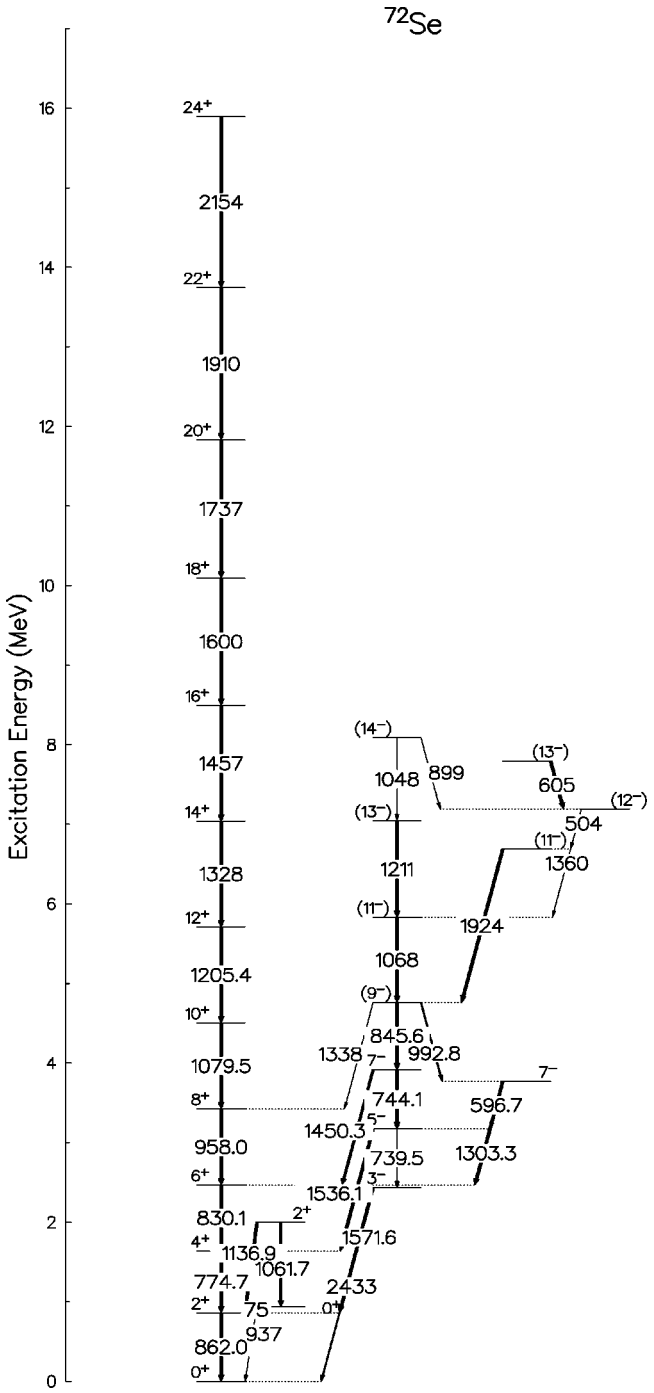

FIG. 1. Partial level scheme of ^{72}Se relevant to the present work.

were collected in the list mode when two or more detectors fired simultaneously. In this arrangement, the Clover detector was used in the add-back mode [14], i.e., it was treated as a single detector and kept at 270° with respect to the beam direction. CS-HPGe detectors were kept in the reaction plane at angles of 15°, 75°, 135°, 225°, and 315° with respect to the beam direction. The background due to radioactivity was reduced with the help of a multiplicity filter consisting of 14 NaI(Tl) detectors. Two-fold coincidences in HPGe/Clover detectors were taken as the start of a time-to-amplitude converter (TAC) and the stop was taken from two-fold (or more) coincidences in the NaI(Tl) multiplicity filter. A 110-nsec-wide prompt window was selected for the time spectrum of the TAC. The single-channel analyzer output of the TAC was taken as the master for coincidence data. The beam intensity was around 3 pnA giving singles rate of $\sim$7 kHz in each HPGe crystals and an event rate of $\sim$100 Hz.

The energy calibration for all the detectors was matched to 0.5 keV/channel. Data were sorted into $4k\times4k$ γ-γ matrices with one of the detectors along the x axis and any of the other detectors along the y axis. The transitions reported in Ref. [9] were identified in our experiment. To get the line-shape spectra of the concerned transitions, their lower gamma transitions were used as gates and these gated spectra were added.

Lifetimes of levels were obtained from the analysis of line shapes in the detectors at 45° and 75°. Line shapes of the transitions obtained were fitted with the program developed by Wells *et al.* [15]. The Monte Carlo simulation technique has been used in this program for the velocity and directional history of a series of recoiling nuclei. Monte Carlo simulation traces both the scattering directions and the velocities of the recoiling ions. The calculations take into account nuclear stopping that leads to large-angle scattering and large energy losses. Shell-corrected Northcliffe and Schilling [16] electronic-stopping-powers have been used. This program obtains a χ^2 minimization of the fit for transition quadrupole moment (Q_t), transition quadrupole moment Q_t(SF) of the modeled side feeding cascade, the intensities of the contamination peak in the region of interest and the normalizing factor to normalize the intensity of the fitted transition. The uncertainties in the measured lifetimes are quoted in Table I for 90% confidence level. We have used rotational cascade side-feeding model that consists of a five-state rotational band with fixed moment of inertia of $\sim 20\hbar^2$ MeV^{-1}. In the present analysis, an effective lifetime was obtained for the 22^+ level by assuming a prompt feed to this state. The side-feeding intensities for all the states in the positive- and negative-parity bands were determined from the γ spectrum obtained at 90°. This gave the side-feeding intensities $\sim$30% for high-spin states and $\sim$20% for the 8^+ and 10^+ states. The side-feeding intensities for the negative-parity states were also found to be $\sim$30%. The fits to the data gave values for the transition quadrupole moments in side-feeding bands $Q_t(\mathrm{SF})=1.6(4)$ e b for the 20^+ state, $Q_t(\mathrm{SF})=2.0(4)$ e b for the 18^+ state, and $Q_t(\mathrm{SF})\sim3.2(4)$ e b for 8^+ to 16^+ states. The transition quadrupole moments for the side-feeding bands for the negative-parity levels were found to be $\sim3.2(4)$ e b from fits to the experimental line shapes. The experimental data along with theoretical fits for γ rays deexciting the 20^+, 16^+, and 11^- levels in ^{72}Se are shown in Fig. 2. The lifetimes obtained in the present work and the earlier measurements [2,11] are listed in Table I. The values obtained in the present work up to the 14^+ level are in good agreement with earlier measurements [2,11]. The adopted values of lifetimes for excited states up to 22^+ are listed in the last column of Table I. The lifetimes of the 16^+, 18^+, 20^+, and 22^+ are also reported. The lifetimes of

TABLE I. Experimental values of lifetimes for excited states in ^{72}Se.

Level energy (keV)	Spin I ($\hbar$)	Transition energy (keV)	τ (ps) Previous work [a]	Present work	Adopted values
861.9	2^+	861.9	4.8(5)		4.8(5)
1636.6	4^+	774.7	3.6(8)		3.6(8)
2476.0	6^+	831.1	2.4(2)		2.4(2)
3424.5	8^+	956.8	0.8(1)	0.60(13)	0.75(8)
4503.9	10^+	1079.4	0.37(5)	0.30(5)	0.34(4)
5709.3	12^+	1205.4	0.20(4)	$0.22^{+0.08}_{-0.06}$	0.21(4)
7037.0	14^+	1327.7	[0.08(3)]	$0.15^{+0.01}_{-0.015}$	0.13(2)
8494.0	16^+	1457.0		0.06(1)	0.06(1)
10094.0	18^+	1600.0		0.060(15)	0.060(15)
11831.0	20^+	1737.0		0.10(2)	0.10(2)
13741.0	22^+	1910.0		<0.07	<0.07
3917.3	7^-	744.0		$0.90^{+0.25}_{-0.30}$	$0.90^{+0.25}_{-0.30}$
4762.8	9^-	845.5		0.85(12)	0.85(12)
5830.8	11^-	1068.0		1.20(15)	1.20(15)
7041.8	13^-	1211.0		<1.0	<1.0

[a]Values given in Ref. [2].

the 4 levels in the negative-parity band are also reported. It will be seen later that these measurements provide crucial information for understanding high-spin behavior of ^{72}Se.

III. DISCUSSION

The aligned angular momentum $I_x(=I-\frac{1}{2})$, kinetic moment of inertia $J^{(1)}$, and dynamic moment of inertia $J^{(2)}$ vs $\hbar\omega$ for the positive-parity band are plotted in Fig. 3. The gradual increment of aligned angular momentum I_x and no sharp backbending is attributed to strong interaction between the yrast-yrare bands [9]. The irregularity in $J^{(2)}$ is observed around $\hbar\omega\approx 0.45$ MeV. The total Routhian surface (TRS) calculations predict three minima—two oblate and one prolate at low spin with $\hbar\omega\leqslant 0.3$ MeV. But only the prolate minimum persists at higher spins. Assuming a prolate deformation $\beta_2=0.33$ and $\gamma=-4°$, the cranked shell model calculations predict the breaking of proton pair at $\hbar\omega=0.45$ MeV and neutron pair breaking at $\hbar\omega=0.50$ MeV. This is in accordance with observed irregularity at frequency $\hbar\omega\approx 0.45$ MeV.

The structure of high-spin states of ^{72}Se was investigated earlier through the microscopic calculations using the EXCITED VAMPIR model [12]. In these calculations, the yrast states of low spins up to 6^+ appear to have mainly an oblate character. For higher spins, an oblate band coexists with many other prolate bands. Altogether, six bands have been calculated up to 22^+. A very complex feeding pattern of medium-spin states was obtained for ^{72}Se, including fast $E2$ and $M1$ transitions. The situation becomes even more complicated because of predicted strong $M1$, $\Delta I=0$ transitions, which in some cases are much faster than intraband $E2$ transitions. A choice of a few ''most probable'' paths of the cascade, leading to the yrast 6^+ state, was made by comparing with the experimental transition strengths. The calculated decay paths involving fast $M1$ transitions between same spins and also transition energies $\geqslant 2.5$ MeV for the $18^+\rightarrow 16^+$ transition were excluded. The transition quadrupole moments obtained for selected cascade of the EXCITED VAMPIR results are plotted in Fig. 4 along with experimental Q_t values listed in Table II. These calculations were performed for mixed oblate and prolate configurations. It is seen that the EXCITED VAMPIR calculations reproduce well the qualitative behavior of the Q_t values with increasing spin. The results indicate a good agreement between the calculated and experimental values for spins up to the 6^+ state and a prolate nature above it. However, the calculated values are relatively lower for spins of 8^+ and 12^+, and also for the 18^+ and 20^+ states. The lowering of Q_t values for some of the spins was interpreted as arising due to dynamical variation of quadrupole and hexadecapole deformations [12].

It is thus considered highly interesting to examine the behavior of these Q_t values for pure oblate or prolate configurations through a model like the PSM [13]. The PSM requires much less numerical effort. Therefore, the calculations are stable and interpretations for their results are easy. The PSM is based on the simple schematic Hamiltonian of the pairing plus quadrupole type given by

$$\hat{H}=\hat{H}_0-\frac{1}{2}\chi\sum_{\mu}\hat{Q}^{\dagger}_{\mu}\hat{Q}_{\mu}-G_M\hat{P}^{\dagger}\hat{P}-G_Q\sum_{\mu}\hat{P}^{\dagger}_{\mu}\hat{P}_{\mu}. \quad (1)$$

H_0 is the spherical single-particle Hamiltonian. The strength of the $\hat{Q}\cdot\hat{Q}$ force parameter χ is adjusted in such a way that the quadrupole deformation ϵ_2 is obtained as a result of the self-consistent HFB procedure. Monopole-pairing strengths used in this calculation are taken from Ref. [10]. Finally, the strength of the quadrupole pairing G_Q is taken proportional to G_M with the proportionality factor of 0.16. We note that

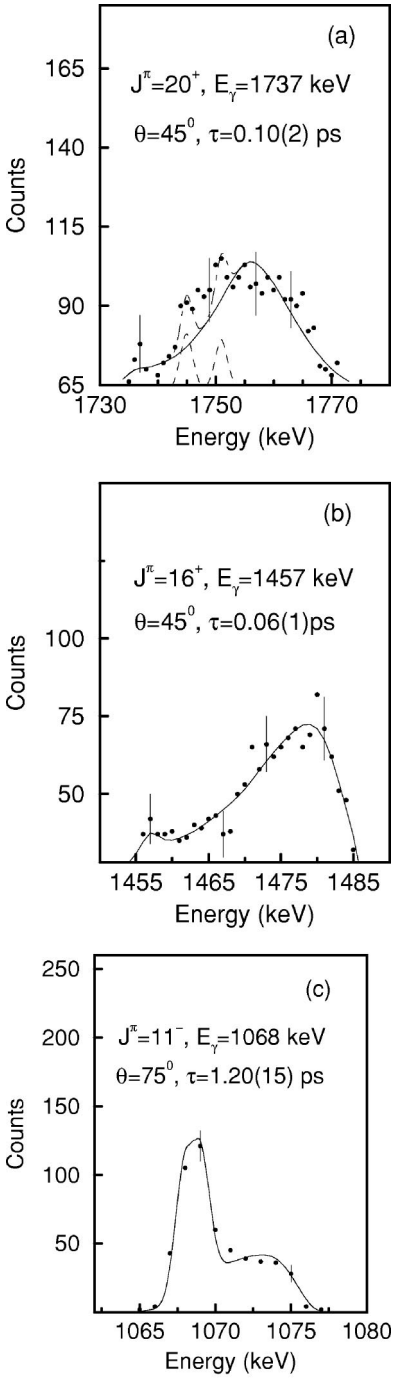

FIG. 2. Experimental and theoretical lineshapes for the (a) 20^{+}, (b) 16^{+}, and (c) 11^{-} levels in ^{72}Se at $\theta=45°$ and 75°. The contaminated peaks in the region of line shape for 1737-keV transition are shown by dashed lines.

the study by Dufour and Zuker [17] has shown explicitly that the residual part of the realistic force is strongly dominated by pairing and quadrupole interactions.

The PSM is a spherical shell model truncated in a Nilsson-BCS single particle basis [13]. The quasiparticle vacuum $|\phi\rangle$ is determined by diagonalization of deformed Nilsson Hamiltonian and a subsequent BCS calculation. For studying nuclei of the mass 80 region, the single-particle space includes $N=2$, 3, and 4 major shells for both neu-

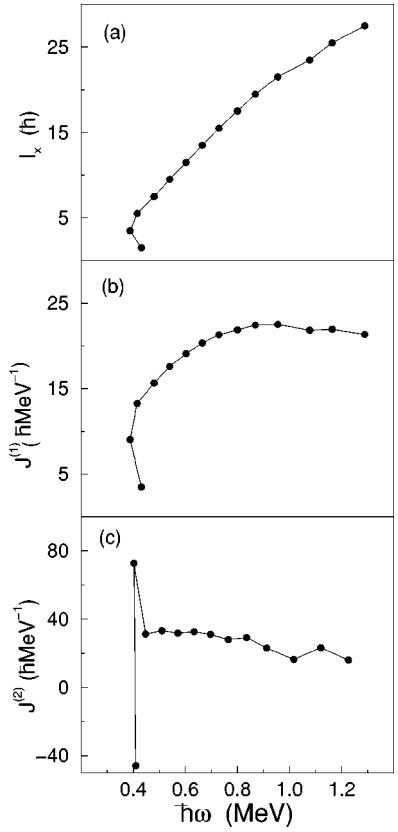

FIG. 3. (a) The aligned quasiparticle angular momentum I_x, (b) the kinematic moment of inertia $J^{(1)}$, and (c) the dynamic moment of inertia $J^{(2)}$ as a function of $\hbar\omega$ for the yrast positive-parity band in ^{72}Se.

TABLE II. Experimental $B(E2)$ and Q_t values for excited states in ^{72}Se.

Level (keV)	Spin I ($\hbar$)	$B(E2)$ (W.u.) [a]	Q_t(Expt.) (eb)
861.9	2^{+}	$20.1^{+2.3}_{-1.9}$	$1.34^{+0.08}_{-0.07}$
1636.6	4^{+}	$45.6^{+13.0}_{-8.3}$	$1.69^{+0.23}_{-0.16}$
2476.0	6^{+}	$48.1^{+4.4}_{-3.7}$	$1.65^{+0.08}_{-0.06}$
3424.5	8^{+}	$76.2^{+9.1}_{-7.3}$	$2.03^{+0.12}_{-0.10}$
4503.9	10^{+}	$92.0^{+12.3}_{-9.7}$	$2.20^{+0.15}_{-0.11}$
5709.3	12^{+}	$85.7^{+20.2}_{-13.7}$	$2.11^{+0.24}_{-0.18}$
7037.0	14^{+}	$85.4^{+15.5}_{-11.4}$	$2.09^{+0.19}_{-0.14}$
8494.0	16^{+}	$116.3^{+23.3}_{-16.6}$	$2.43^{+0.23}_{-0.18}$
10094.0	18^{+}	$72.8^{+24.3}_{-14.7}$	$1.92^{+0.29}_{-0.21}$
13741.0	20^{+}	$29.0^{+7.3}_{-4.8}$	$1.21^{+0.14}_{-0.11}$
15651.0	22^{+}	>25.7	>1.13
391.37	7^{-}	$122.0^{+61.0}_{-27.0}$	$3.32^{+0.78}_{-0.38}$
4762.8	9^{-}	$98.0^{+16.0}_{-12.0}$	$2.62^{+0.21}_{-0.17}$
5830.8	11^{-}	$25^{+4.0}_{-3.0}$	$1.25^{+0.09}_{-0.07}$
7041.8	13^{-}	>22.0	>1.12

[a] 1 W.u. = 17.8 e^2fm^4.

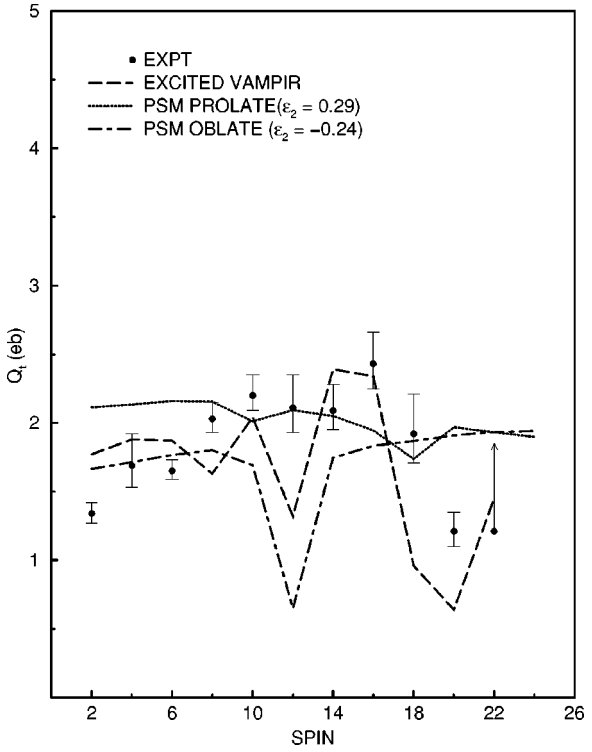

FIG. 4. Comparison of the measured transition quadrupole moments Q_t for excited states in ^{72}Se with the predictions of PSM and EXCITED VAMPIR model. The PSM is calculated with a prolate shape $\epsilon_2=0.29$ and an oblate shape $\epsilon_2=-0.24$.

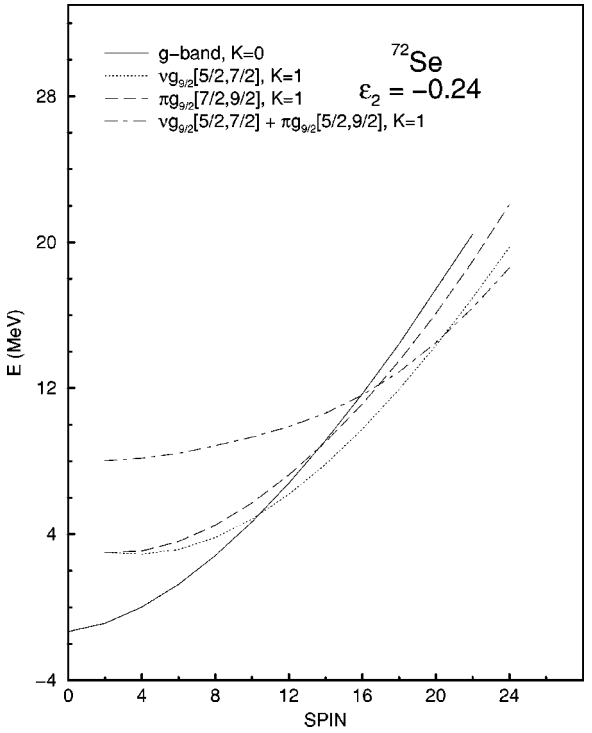

FIG. 5. Band diagram of ^{72}Se for an oblate shape with $\epsilon_2=-0.24$.

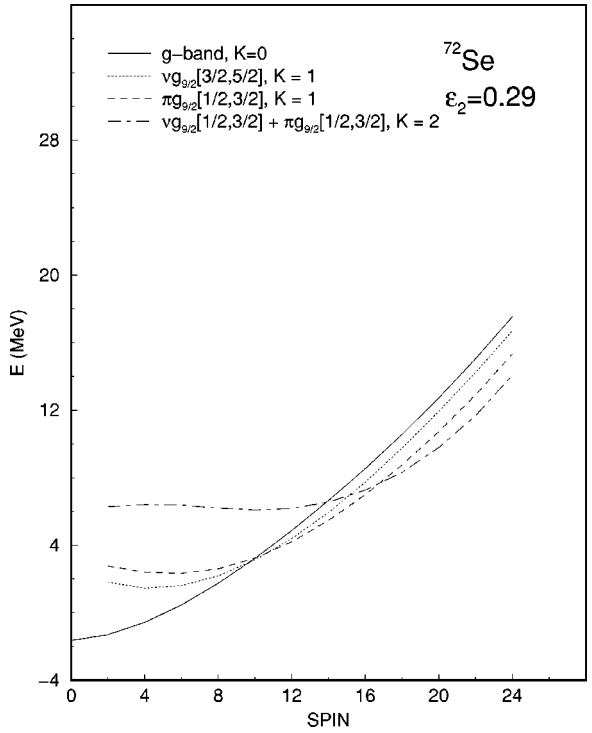

FIG. 6. Band diagram of ^{72}Se for a prolate shape with $\epsilon_2=0.29$.

trons and protons. The shell model basis is constructed by including the vacuum and the lower-lying two-quasiparticle (2-qp) and four-quasiparticle (4-qp) states. The rotational symmetry of these deformed states is restored by standard projection technique to form the spherical basis in the laboratory frame. This basis is used to diagonalize the shell model Hamiltonian given by Eq. (1). The details can be found in the recent systematical study of even-even mass-80 nuclei by the PSM [18].

In the present work, bands in ^{72}Se are calculated for a fixed oblate deformation $\epsilon_2=-0.24$ and a prolate deformation $\epsilon_2=0.29$ corresponding to the minima obtained in the TRS calculations mentioned earlier. The important configurations for the oblate deformation with $\epsilon_2=-0.24$ and the prolate deformation of $\epsilon_2=0.29$, are shown in Fig. 5 and Fig. 6, respectively. These are so-called band diagrams [13]. It can be seen in Fig. 5 that the neutron 2-qp state involving [422]5/2 and [413]7/2 orbitals crosses sharply the ground band between $I=10$ and 12. After that, this 2-qp state remains the lowest in energy and is the main component of the yrast band in this nucleus. On the other hand, proton 2-qp state lies higher in energy, thus plays a less role in the yrast band. This sharp band crossing by a single 2-qp band leads generally to a larger effect. In contrast, Fig. 6 shows a simultaneous crossing of the proton 2-qp band based on the configuration involving [440]1/2 and [431]3/2 orbitals and the neutron 2-qp band involving [431]3/2 and [422]5/2 orbitals. Together with the ground band, a picture of band interaction within three bands is seen between $I=10$ and 12. In this case, the effective band interaction is much stronger as explicitly discussed in Ref. [13]. This picture is consistent with the early understanding about the gradual alignment of 2-qp

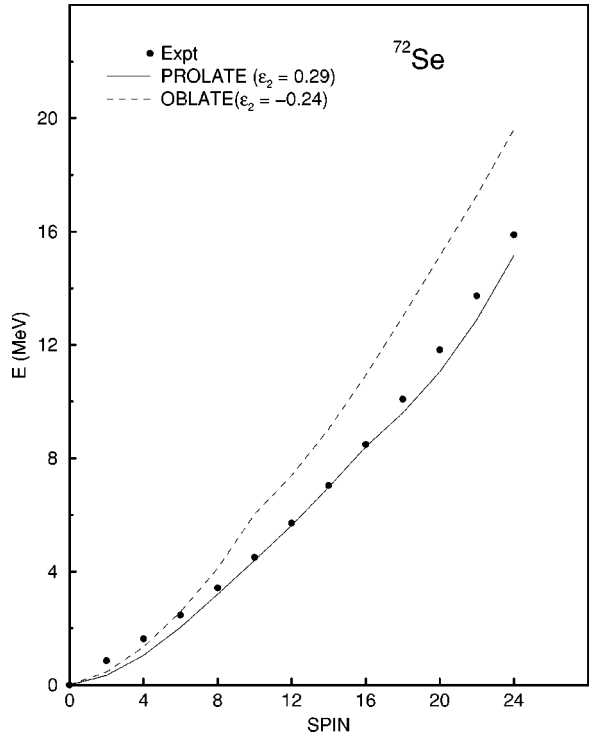

FIG. 7. Comparison of experimental energies of the yrast levels in ^{72}Se with the calculated energies for a prolate shape with $\epsilon_2 = 0.29$ and oblate shape with $\epsilon_2 = -0.24$.

pairs [9]. Around $I = 18$ to 20, the decoupled 4-qp band with $K = 2$ (see Fig. 6 for its configuration) crosses the 2-qp bands and starts contributing maximum to the yrast states.

The calculated yrast energies based on the oblate and prolate configurations, separately, are compared with the experimental energies of the yrast levels in Fig. 7. One can see that the calculations using the oblate mean field gives better agreement compared to the prolate mean field for the spin states of $I \leqslant 6$. On the other hand, a better agreement is obtained with the prolate mean field for $I > 6$. These PSM results are satisfactory for a description of a transitional nucleus with various shapes.

Transition quadrupole moments Q_t obtained from the PSM calculations for both the oblate and the prolate mean fields are also plotted in Fig. 4. At lower spins, i.e., $I \leqslant 6$, results with the oblate mean field reproduce the experimental values, but the calculated values are very different from the experimental numbers for the high-spin states. In particular, the sudden drop in Q_t at $I = 12$ is not supported by the data. This drop has its source as the sudden structure change in the yrast wave function that is caused by the sharp band crossing discussed in Fig. 5. In Fig. 4, similar disagreement with data at $I = 12$ can also be seen from the early EXCITED VAMPIR results. The transition quadrupole moments calculated by the PSM with the prolate mean field give very good agreement with all the experimental Q_t values above $I = 6$ except for $I = 20$. Thus, the experimental Q_t values along with the PSM calculations, support the oblate deformation for low spins with $I \leqslant 6$ and the prolate deformation for $I > 6$ in ^{72}Se.

The negative-parity band in this region is characterized by strong deformation and octupole vibrational phonon coupled

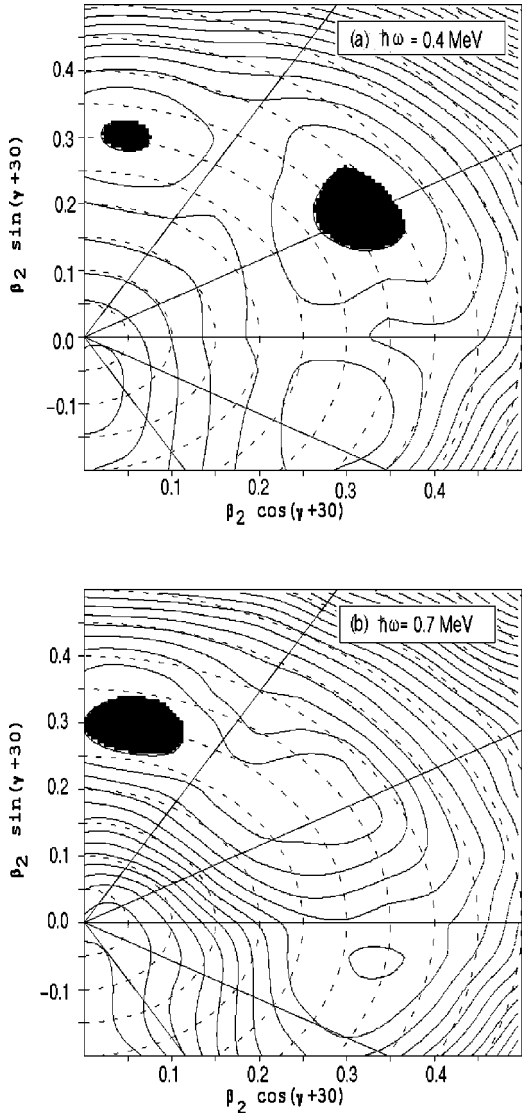

FIG. 8. Total Routhian surface plots in the β_2-γ plane for the negative-parity odd-signature quasiproton band in ^{72}Se for two rotational frequencies $\hbar\omega = 0.4$ MeV and 0.7 MeV are shown in (a) and (b), respectively. The energy separation between the contours is 250 keV.

to the rotational bands [19]. Measured Q_t values for the negative-parity band show a continuous drop with increasing spin (see Table II). The shape for the negative-parity band for ^{72}Se has been calculated as a function of rotational frequencies in the cranked Hartree-Fock-Bogoliubov model with the Woods-Saxon potential and the monopole pairing force [20,21] to understand the observed drop in Q_t values. In these calculations, the pairing term was calculated by solving the BCS gap equation at rotational frequency $\omega = 0$ using the interaction strength G obtained from systematics. The pairing gap Δ was allowed to vary smoothly as a linear function of ω in such a way that it becomes $\Delta_0/2$ at the critical frequency ω_c, where Δ_0 is the pair gap at $\omega = 0$. $\hbar\omega_c^{\pi} = 1.15$ MeV for proton and $\hbar\omega_c^{\nu} = 0.95$ MeV for neutron are taken for nuclei in this mass region. The TRS was calculated in a β_2-γ mesh for the negative-parity odd-

signature quasiproton band. These are calculated at various rotational frequencies and the total energy is minimized with respect to the hexadecapole deformation parameter β_4 for each value of (β_2, γ). The TRS results were plotted in Fig. 8 for two frequencies $\hbar\omega = 0.4$ and 0.7 MeV. It can be seen that there are two minima within 250 keV energy difference for $\hbar\omega = 0.4$ MeV. One of them is the collective prolate with $\beta_2 = 0.35, \gamma = 0°$ and the other is the noncollective oblate with $\beta_2 = 0.30, \gamma = 60°$. The noncollective shape with $\beta_2 = 0.3, \gamma = 54°$ stabilizes at higher frequencies. The decrease of measured Q_t values can thus be attributed to the stabilization of noncollective shape.

IV. CONCLUSION

Lifetimes of the high spin states were measured up to highest possible spins along the yrast positive-parity, as well as the negative-parity bands. The transition quadrupole moments obtained from the measured lifetimes were compared with the predictions of different models. For the positive-parity band, the EXCITED VAMPIR model predicted qualitatively well the observed variation in transition quadrupole moment Q_t with increasing spin through the dynamical changes in intrinsic quadrupole and hexadecapole moments. It, however, produced much deeper minima at $I = 12$ and $I \sim 18-20$ than the observed experimentally. On the other hand, the PSM calculations in the present work neatly confirmed the oblate deformation at lower spins with $I \leqslant 6$ and a transition to the prolate shape at higher spins, but it produced smaller dips around the second band crossing. Both calculations and experimental data are, however, consistent with the conclusion of an oblate character of ^{72}Se at lower spins and a stabilization towards prolate shape with dynamical changes in deformation at high spins. The negative-parity band seems to favor noncollective shape. However, detailed investigations of the structure of the high spin region in ^{72}Se in search of the fast $M1$ transitions predicted by the EXCITED VAMPIR calculations are still needed.

ACKNOWLEDGMENTS

We gratefully acknowledge the help of all the pelletron staff for smooth functioning of the accelerator. We are thankful to Dr. V. Nanal for her help during the beam time. We are grateful to Dr. G. Mukherjee for TRS calculations. One of us (Y.S.) thanks Professor G.-L. Long for his warm hospitality and for the support from the China National Science Foundation under Contract No. 19775026 and the senior visiting scholar program of Tsinghua University.

[1] R. Bengtsson, P. Möller, J. R. Nix, and J. Zhang, Phys. Scr. **29**, 402 (1984).
[2] K. P. Lieb and J. J. Kolata, Phys. Rev. C **15**, 939 (1977).
[3] J. H. Hamilton, A. V. Ramayya, W. T. Pinkston, R. M. Ronningen, G. Garcia-Bermudez, H. K. Carter, R. L. Robinson, H. J. Kim, and R. O. Sayer, Phys. Rev. Lett. **32**, 239 (1974).
[4] H. P. Hellmeister, E. Schmidt, M. Uhrmacher, R. Rascher, K. P. Lieb, and D. Pantelica, Phys. Rev. C **17**, 2113 (1978).
[5] V. G. Kiptilyi, I. Kh. Lemberg, A. S. Mishin, and A. A. Pasternak, Bull. Acad. Sci. USSR, Phys. Ser. (Engl. Transl.) **43**, 26 (1979).
[6] J. Adam, M. Honusek, A. Spalek, D. N. Doynikov, A. D. Efimov, M. F. Kudojarov, I. Kh. Lemberg, A. A. Pasternak, O. K. Vorov, and U. Y. Zhovliev, Z. Phys. A **332**, 143 (1989).
[7] M. Wiosna, J. Busch, J. Eberth, M. Liebchen, T. Mylaeus, N. Schmal, R. Sefzig, S. Skoda, and W. Teichert, Phys. Lett. B **200**, 255 (1988).
[8] G. Mukherjee, P. Joshi, S. N. Roy, S. Datta, R. P. Singh, S. Muralithar, and R. K. Bhowmik, Z. Phys. A **359**, 111 (1997).
[9] T. Mylaeus, J. Busch, J. Eberth, M. Liebchen, R. Sefzig, S. Skoda, W. Teichert, M. Wiosna, P. von Brentano, K. Schiffer, K. O. Zell, A. V. Ramayya, K. H. Maier, H. Grawe, A. Kluge, and W. Nazarewicz, J. Phys. G **15**, L135 (1989).
[10] J. Döring, G. D. Johns, M. A. Riley, S. L. Tabor, Y. Sun, and J. A. Sheikh, Phys. Rev. C **57**, 2912 (1998).
[11] J. Heese, K. P. Lieb, L. Luhmann, F. Raether, B. Wormann, D. Alber, H. Grawe, J. Eberth, and T. Mylaeus, Z. Phys. A **325**, 45 (1986).
[12] A. Petrovici, K. W. Schmid, F. Grummer, and A. Faessler, Nucl. Phys. **A504**, 277 (1989).
[13] K. Hara and Y. Sun, Int. J. Mod. Phys. A **4**, 637 (1995).
[14] P. K. Joshi, H. C. Jain, A. S. Medhi, S. Chattopadhyay, S. Bhattacharya, and A. Goswamy, Nucl. Instrum. Methods Phys. Res. A **399**, 51 (1997).
[15] J. C. Wells *et al.*, Report No. ORNL/TM-9105, 1985 (unpublished).
[16] N. C. Northcliffe and Schilling, Nucl. Data, Sect. A **7**, 233 (1970).
[17] M. Dufour and A. P. Zuker, Phys. Rev. C **54**, 1641 (1996).
[18] R. Palit, J. A. Sheikh, Y. Sun, and H. C. Jain (unpublished).
[19] P. D. Cottle, J. W. Holcomb, T. D. Johnson, K. A. Stuckey, S. L. Tabor, P. C. Womble, S. G. Buccino, and F. E. Durham, Phys. Rev. C **42**, 1254 (1990).
[20] W. Nazarewicz, J. Dudek, R. Bengtsson, T. Bengsson, and I. Rangarsson, Nucl. Phys. **A435**, 397 (1985).
[21] W. Nazarewicz, M. A. Riley, and J. D. Garrett, Nucl. Phys. **A512**, 61 (1990).